

See discussions, stats, and author profiles for this publication at: <https://www.researchgate.net/publication/231666941>

Unraveling the Formation of Core–Shell Structures in Nanoparticles by S-XPS

ARTICLE *in* JOURNAL OF PHYSICAL CHEMISTRY LETTERS · FEBRUARY 2010

Impact Factor: 7.46 · DOI: 10.1021/jz100049z

CITATIONS

13

READS

48

4 AUTHORS, INCLUDING:



Fabiano Bernardi

Universidade Federal do Rio Grande do Sul

25 PUBLICATIONS 289 CITATIONS

[SEE PROFILE](#)



Gerhard H. Fecher

Max Planck Institute for Chemical Physics of...

260 PUBLICATIONS 5,280 CITATIONS

[SEE PROFILE](#)

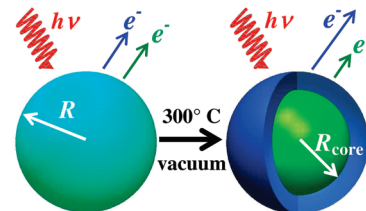
Unraveling the Formation of Core–Shell Structures in Nanoparticles by S-XPS

Fabiano Bernardi,[†] Gerhard H. Fecher,[‡] Maria C. M. Alves,[§] and Jonder Morais^{*,†}

[†]Instituto de Física, Universidade Federal do Rio Grande do Sul (UFRGS), Avenida Bento Gonçalves, 9500, Bairro Agronomia, CP 15051, CEP 91501-970, Porto Alegre, RS, Brazil, [‡]Institut für Anorganische und Analytische Chemie - Johannes Gutenberg Universität, 55099 Mainz, Germany, and [§]Instituto de Química, Universidade Federal do Rio Grande do Sul (UFRGS), Avenida Bento Gonçalves, 9500, Bairro Agronomia, CP 15003, CEP 91501-970, Porto Alegre, RS, Brazil

ABSTRACT The combination of the surface sensitivity of X-ray photoelectron spectroscopy (XPS) with the high flux and variable photon energy excitation of Synchrotron radiation (S-XPS) is used to probe the atomic distribution of bimetallic nanoparticles. Based on the energy dependence of the photoemission differential cross section of core level photoelectrons, we propose a methodology to monitor the formation and to evaluate sizes of the core–shell structure. We have successfully applied it to unveil the mechanism involved in the atomic rearrangement of thermally treated Pt_{0.7}Pd_{0.3} nanoparticles.

SECTION Nanoparticles and Nanostructures



The determination of the atomic arrangement in nanoparticles has attracted great interest^{1–3} mainly due to its strong influence on the final properties of the nanoparticles, which is very attractive for different areas of research. For catalysis, the use of bimetallic over monometallic nanoparticles is quite appealing, as the addition of a second metal provides a method to tailor catalytic activity and selectivity through cooperative effects.^{4,5} Since catalytic processes are highly dependent on surface properties, much effort has been dedicated to control the population of surface atoms rather than inner atoms,⁶ hence the atomic distribution within the bimetallic nanoparticles plays an important role. Among all possible atomic arrangements, the so-called core–shell structure has been the subject of many studies from both experimental and theoretical point of views, since it is possible to enhance or to design new physical and chemical properties that may not be obtained in single-component nanoparticles.^{7–14} It is also possible, by modifying the thickness of the shell, to tailor these properties within a certain range. It is well-known that gold is inert for the hydrogenation of hex-2-yne to cis-hex-2-ene; however, Schmid et al.¹⁵ demonstrated that a palladium core, 20 nm in size, covered with a very thick gold shell (4–18 nm) is much more reactive than pure Pd nanoparticles (20 nm) for this same catalytic reaction.

The core–shell formation may be investigated by several techniques, but traditionally the microscopy methods (transmission electron (TEM), scanning electron (SEM), scanning tunneling (STM), and atomic force (AFM) microscopies) are applied to identify the particle structure and size.⁶ X-ray-based characterization methods are very useful to obtain more detailed information on the atomic arrangement and surface composition of nanosystems.^{16,17} Particularly, photoelectron spectroscopy excited by tunable

Synchrotron radiation (S-XPS) allows the variation of the sampling depth. This is due to the well-known dependence of the electron mean free path on its kinetic energy.¹⁸ In a core–shell structure, the core signal is screened by the shell at low photoelectron kinetic energies and becomes gradually more dominant when the excitation energy is increased, enlarging the photoelectron mean free path. This technique was employed to study the depth distribution of In and Zn atoms in InP core–ZnS shell nanoparticles using soft X-rays.¹⁶ The use of S-XPS is advantageous in the case of nanoparticles with an approximately spherical geometry, where angle-resolved XPS measurements cannot be successfully applied.

In comparison with other bimetallic systems, the combination of platinum and palladium is particularly advantageous in catalysts, where it is used for hydroisomerization, hydrocracking, hydrogenation, and hydrotreatment.¹⁹ It has been proposed that its catalytic properties are connected to surface atomic segregation effect, which was experimentally observed in supported Pt–Pd catalysts.^{19–21} There are also many theoretical studies about surface segregation in the literature;^{11,22–27} however, few studies have addressed non-supported Pt–Pd nanoparticles.^{7,9,12,13} In a recent study,⁹ we demonstrated that Pd migrates toward the surface in non-supported Pt_xPd_{1-x} ($x = 1, 0.7$, or 0.5) nanoparticles submitted to hydrogen reduction and posterior sulfidation, and that the presence of Pd inhibits the sintering of a dispersed Pt phase in the alloy samples. Despite all the published results, there is still a major issue as to whether

Received Date: January 14, 2010

Accepted Date: February 10, 2010

the atomic rearrangement effect is thermally driven or induced by the gas phase reaction, i.e., reaction-driven.

In this letter we present a clear experimental methodology on the use of S-XPS to investigate the atomic arrangement of nanoparticles, based on the knowledge of the photoemission differential cross section and the mean free path of the photoelectrons for the selected photon energy excitation. We apply this method to the case of $\text{Pt}_{0.7}\text{Pd}_{0.3}$ nanoparticles submitted to a thermal treatment, without the influence of a gaseous atmosphere. The samples were annealed in vacuum at 300 °C, for 20 and 50 min. We observe an atomic rearrangement of Pt and Pd atoms inside the nanoparticles, leading to a core–shell structure, corroborating a thermally induced effect. On the basis of the S-XPS results, we estimate the core radius and the shell thickness of the annealed nanoparticles.

XP spectra were collected for the as-prepared sample as well as after two thermal treatments at 300 °C: first, after 20 min of annealing and another measurement after 50 min. These treatments were performed in a preparation chamber at a pressure at about 1.5×10^{-6} mbar and a temperature raising rate of 30 °C/min. The overall treatment time was

chosen to be equivalent to those used in our previous study⁹ for samples that were treated under various gaseous atmospheres (He, H₂, and H₂S).

In this work, we propose the use of S-XPS to estimate the core radius R_{core} and the shell thickness t , supposing that the nanoparticles have an ideal core–shell structure. The area measured under a photoemission peak I is given by

$$I = 4\pi FS(E_{\text{kin}}) \frac{d\sigma}{d\Omega}(E_{\text{ph}}) \int_0^R r^2 \rho(r) \exp\left(\frac{-r}{\lambda(E_{\text{kin}}) \cos \theta}\right) dr \quad (1)$$

where F is the X-ray flux on the sample, $S(E_{\text{kin}})$ is the spectrometer efficiency for detecting the photoelectron at kinetic energy E_{kin} , $d\sigma(E_{\text{ph}})/d\Omega$ is the differential cross section, E_{ph} is the photon energy, $\rho(r)$ is the atomic density, $\lambda(E_{\text{kin}})$ is the electron mean free path at kinetic energy E_{kin} , R is the nanoparticle radius, and θ is the takeoff angle (in this case $\theta = 45^\circ$).

Calculating $d\sigma(E_{\text{ph}})/d\Omega$ and integrating eq 1 considering the Pt 4f and Pd 3d photoelectrons, an analytical expression to cross section corrected peak area ratio, A , is obtained (eq 2):

$$A = \frac{I_{\text{Pt}4f} \left[\frac{d\sigma^{\text{Pd}5d}}{d\Omega}(E_{\text{ph}}) \right]}{I_{\text{Pd}3d} \left[\frac{d\sigma^{\text{Pt}4f}}{d\Omega}(E_{\text{ph}}) \right]} \\ = \left(\frac{\rho(r)^{\text{Pt}}}{\rho(r)^{\text{Pd}}} \right) \frac{\left\{ 2\lambda^*(E_{\text{kin}}^{\text{Pt}4f})^3 - \lambda^*(E_{\text{kin}}^{\text{Pt}4f}) \exp\left[\frac{-R_{\text{core}}}{\lambda^*(E_{\text{kin}}^{\text{Pt}4f})}\right] [R_{\text{core}}^2 + 2\lambda^*(E_{\text{kin}}^{\text{Pt}4f}) R_{\text{core}} + 2\lambda^*(E_{\text{kin}}^{\text{Pt}4f})^2] \right\}}{\left\{ \lambda^*(E_{\text{kin}}^{\text{Pd}5d}) \exp\left[\frac{-R_{\text{core}}}{\lambda^*(E_{\text{kin}}^{\text{Pd}5d})}\right] [R_{\text{core}}^2 + 2\lambda^*(E_{\text{kin}}^{\text{Pd}5d}) R_{\text{core}} + 2\lambda^*(E_{\text{kin}}^{\text{Pd}5d})^2] - \lambda^*(E_{\text{kin}}^{\text{Pd}5d}) \exp\left[\frac{-R}{\lambda^*(E_{\text{kin}}^{\text{Pd}5d})}\right] [R^2 + 2\lambda^*(E_{\text{kin}}^{\text{Pd}5d}) R + 2\lambda^*(E_{\text{kin}}^{\text{Pd}5d})^2] \right\}} \quad (2)$$

The same value of $S(E_{\text{kin}})$ is used for photoelectrons from Pt 4f and Pd 3d levels and $\lambda^* \equiv \lambda \cos \theta$. The integration is made between the limits 0 and R_{core} for Pt 4f photoelectrons and R_{core} and R for Pd 3d photoelectrons, since we are supposing the existence of an ideal core–shell structure. In this case, $\rho(r)^{\text{Pt}} = 0$ in the shell region ($R_{\text{core}} < r < R$) and $\rho(r)^{\text{Pd}} = 0$ in the core region ($0 < r < R_{\text{core}}$). The evolution of the experimental values of $I_{\text{Pt}4f}$ and $I_{\text{Pd}3d}$, and consequently of A , allows the evaluation of the changes in the Pt and Pd depth distribution and the calculation of the R_{core} value from the expression above, considering that no sintering effect has occurred.

TEM results of the $\text{Pt}_{0.7}\text{Pd}_{0.3}$ nanoparticles (Figure 1) show that their mean diameter is (5.3 ± 1.2) nm. Figure 2 displays high-resolution TEM (HRTEM) micrographs for $\text{Pt}_{0.7}\text{Pd}_{0.3}$ nanoparticles (a) before and (b) after thermal treatment at 300 °C for 50 min and the corresponding Fourier transform (FT) patterns. Since the difference in the lattice constant between Pd and Pt is very small (0.03 Å), it is not possible to assign these FT patterns to the Pt or Pd crystal lattice.

Pd 3d photoemission spectra for the as-prepared and annealed $\text{Pt}_{0.7}\text{Pd}_{0.3}$ nanoparticles, obtained at different photon energies ($E_{\text{ph}} = 1840$ eV and $E_{\text{ph}} = 2800$ eV), are displayed in Figure 3. The as-prepared sample displays the Pd 3d_{5/2} and Pd 3d_{3/2} doublet as well as the Pt 4d_{3/2} (332.0 eV). The binding energy values for the Pd 3d_{5/2} chemical components correspond to Pd–Pd bonds (at 335.2 eV) and palladium oxide (PdO) (336.4 eV).⁹ The Pt 4f_{7/2} and Pt 4f_{5/2} doublet (not shown here) presents binding energies $E_b = 70.8$ and 74.1 eV, associated to Pt–Pt bonds. The wider full width at half-maximum (fwhm) for the spectra obtained with $E_{\text{ph}} = 2800$ eV is due to a lower energy resolution of the beamline monochromator at higher energies. After annealing, no changes are observed in the chemical composition.

The FT patterns shown in Figure 2a of the central (1a) and external (2a) regions present no significant difference. The HRTEM image of Figure 2b gives distinct FT for the regions 1b and 2b, which is due to different crystalline orientations in the regions that constitute the nanoparticles. The change in

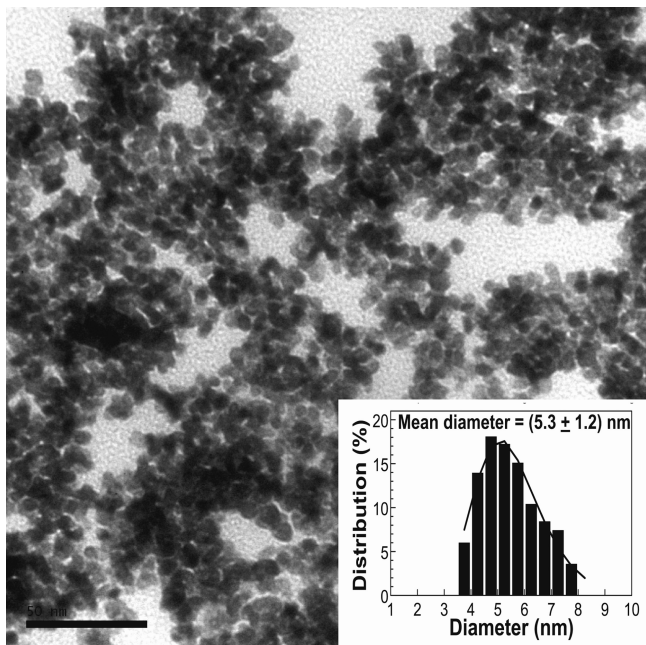


Figure 1. TEM image and histogram (inset) showing the particle size distribution of $\text{Pt}_{0.7}\text{Pd}_{0.3}$ nanoparticles. The solid line in the histogram represents the monomodal function used to adjust the diameter distribution of the nanoparticles. The scale bar dimension is 50 nm.

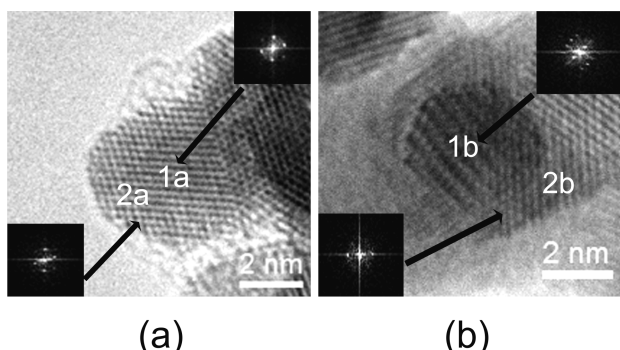


Figure 2. Experimental HRTEM images of $\text{Pt}_{0.7}\text{Pd}_{0.3}$ nanoparticles (a) before and (b) after thermal treatment at $300\text{ }^\circ\text{C}$ for 50 min. The insets represent the FT of the region indicated by the arrow.

the crystalline orientation indicates the existence of a core (1b) and shell (2b) region in the nanoparticle subjected to the thermal treatment. The capping of the Pt core by the Pd shell could be evidenced by a well-known optical effect called Moiré fringe that can be seen in region 1b of Figure 2b. The association of a core–shell structure with the existence of a Moiré pattern in the core region was already reported in the literature.^{14,28,29} The HRTEM image of a core–shell Pt–Pd nanoparticle generally shows a negligible contrast between the core and the shell regions.² Despite this difficulty, there is an indication of the core–shell structure due to the difference of orientation in both regions and the formation of Moiré fringes in the core region.

The modifications in the XPS peak's relative intensity are better visualized with the aid of Table 1, which presents

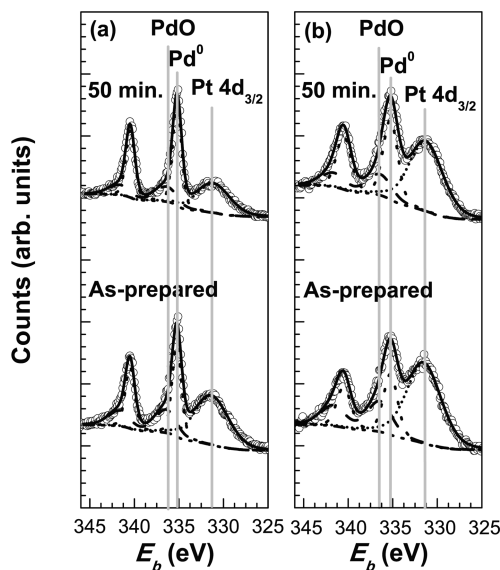


Figure 3. Pd 3d XPS regions for (a) $E_{\text{ph}} = 1840\text{ eV}$ and (b) $E_{\text{ph}} = 2800\text{ eV}$ for the as-prepared $\text{Pt}_{0.7}\text{Pd}_{0.3}$ nanoparticles and treated to $300\text{ }^\circ\text{C}$ during 50 min. The vertical lines indicate the binding energies of the chemical components. All the spectra are presented with the same x and y -scale, along with their fitting curves.

Table 1. Experimental Values for the Cross Section Corrected Peak Area Ratio Obtained from the XPS Fitting for the As-Prepared $\text{Pt}_{0.7}\text{Pd}_{0.3}$ Nanoparticles, after Thermal Treatment at $300\text{ }^\circ\text{C}$ for 20 and 50 min

	$A = \text{Pt 4f/Pd 3d}$	
	$E_{\text{ph}} = 1840\text{ eV}$	$E_{\text{ph}} = 2800\text{ eV}$
as-prepared	1.43 ± 0.04	1.43 ± 0.08
$T = 300\text{ }^\circ\text{C}, 20\text{ min}$	1.07 ± 0.06	1.21 ± 0.07
$T = 300\text{ }^\circ\text{C}, 50\text{ min}$	1.03 ± 0.04	1.23 ± 0.09

a quantification of the Pt 4f/Pd 3d peak area ratio, normalized by the calculated $d\sigma(E_{\text{ph}})/d\Omega$ values (see details in the Supporting Information). From the values presented in Table 1, one observes that A is the same at both incident photon energies for the as-prepared samples. After the thermal treatments (20 and 50 min) A decreases for $E_{\text{ph}} = 1840\text{ eV}$. These results suggest that, in the as-prepared samples, the Pt and Pd atoms have no preferential site inside the nanoparticles. The decrease in the A value after the thermal treatment in vacuum implies that there is a Pd migration toward the surface of the nanoparticles. The core–shell formation occurs mainly in the first 20 min, since the A value for thermal treatment after 20 and 50 min are similar. For $E_{\text{ph}} = 2800\text{ eV}$, the decrease in the A value after thermal treatment is less significant than that for $E_{\text{ph}} = 1840\text{ eV}$. This is associated with a larger probing depth at $E_{\text{ph}} = 2800\text{ eV}$ due to the higher kinetic energy of the photoelectrons. In this case, the XPS signal is less sensitive to surface changes. We have previously observed the core–shell formation on nanoparticles submitted to hydrogen reduction or sulfidation processes in similar conditions of temperature and time.⁹

Applying the A value from Table 1 for $E_{\text{ph}} = 1840\text{ eV}$, the electron mean free path from the TPP-2 M formula¹⁸ and the

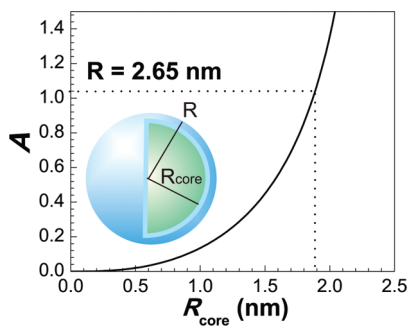


Figure 4. Theoretical values for the R_{core} dependence of the cross section corrected peak area ratio, A , for $\text{Pt}_{0.7}\text{Pd}_{0.3}$ nanoparticles with radius of $R = 2.65 \text{ nm}$ (from Figure 1). The dotted lines indicate the A and the corresponding R_{core} obtained for the samples treated for 50 min.

Table 2. Comparison between the R_{core} and Thickness t Obtained in This Work with the Calculated Values for $\text{Pt}_{0.7}\text{Pd}_{0.3}$ Nanoparticles Submitted to Hydrogen Reduction and Posterior Sulfidation at 300°C^9

	R_{core} (nm)	t (nm)
$\text{Pt}_{0.7}\text{Pd}_{0.3}$ 300°C , 20 min (this work)	1.9	0.8
$\text{Pt}_{0.7}\text{Pd}_{0.3}$ 300°C , 50 min (this work)	1.9	0.8
$\text{Pt}_{0.7}\text{Pd}_{0.3}$ 300°C , reduced	1.9	0.8
$\text{Pt}_{0.7}\text{Pd}_{0.3}$ 300°C , sulfidized	1.1	1.6

average nanoparticle radius from TEM measurements ($R = 2.65 \text{ nm}$) in eq 2, an R_{core} value of $(1.9 \pm 0.2) \text{ nm}$ is obtained. Consequently, the nanoparticles would have a shell thickness t of $(0.8 \pm 0.2) \text{ nm}$. Figure 4 shows the A dependence on the R_{core} . Using the equivalent values at $E_{\text{ph}} = 2800 \text{ eV}$, we obtain a quite similar R_{core} value of $(2.1 \pm 0.2) \text{ nm}$. The difference is within the experimental error. On the basis of the HRTEM image (Figure 2b) we can estimate the R_{core} value of 1.78 nm , which is consistent with those established from the S-XPS measurements.

We have used the same method described above to calculate R_{core} and thickness t for the $\text{Pt}_{0.7}\text{Pd}_{0.3}$ nanoparticles studied previously,⁹ where a core–shell formation was observed after reduction and sulfidation processes. Those S-XPS data were collected using $E_{\text{ph}} = 1840 \text{ eV}$, and the results are presented in Table 2. The same value of R_{core} ($\approx 1.9 \text{ nm}$) is obtained for samples thermally treated in vacuum (300°C , 20 min) or in H_2 (300°C , 20 min) atmosphere. For the sulfidated sample,⁹ the R_{core} radius decreases, resulting in a thicker shell due to the incorporation of sulfur in the nanoparticles. With these results, we clarify that the core–shell formation in $\text{Pt}_{0.7}\text{Pd}_{0.3}$ nanoparticles is a thermally driven process.

Surface segregation induced by thermal treatment under hydrogen^{20,30} atmosphere was observed for Pt–Pd alloys. Szabo et al.³⁰ used a model taking the top five surface layers into account to estimate the influence of hydrogen absorption on the surface composition of $\text{Pt}_{0.7}\text{Pd}_{0.3}$ alloys. They predicted an increase in Pd surface segregation. Nevertheless, our results show that thermal treatment in H_2 resulted in the same core–shell structure as the treatment in vacuum, both cases during 20 min.

For the $\text{Pd}_{0.5}\text{Rh}_{0.5}$ nanoparticles, Tao et al.⁷ observed a reversible segregation of Rh and Pd under alternating atmospheres (NO , CO , O_2 and H_2) at 300°C by in situ XPS. The authors did not observe the atomic rearrangement for as-prepared $\text{Pt}_{0.5}\text{Pd}_{0.5}$ core–shell nanoparticles under different atmospheres (NO , $\text{NO} \pm \text{CO}$ and CO) at 300°C . The system maintained a Pt-rich core and a Pd-enriched shell without substantial segregation of Pt atoms during the employed reactions.

The presence of Pd atoms at the surface of Pt–Pd nanoparticles is expected from a theoretical point of view.^{23,25,26} This is due to the lower surface free energy γ of Pd and the higher cohesive energy of Pt.²⁵ The surface segregation of Pd atoms has been shown experimentally in the literature.^{7,9,19–21} Experimental values obtained for the $\text{Pt}_{0.8}\text{Pd}_{0.2}$ bulk alloy indicate that the heat of segregation Q_{seg} of Pd is 11.5 kJ/mol , with increasing Q_{seg} values for higher Pd contents.²⁰ On the basis of the dependence of the Q_{seg} on the composition,²⁰ we roughly estimated the Q_{seg} of 12 kJ/mol for $\text{Pt}_{0.7}\text{Pd}_{0.3}$ bulk alloy. In this study, only 7 kJ/mol is transferred to the system with the employed thermal treatment. Despite the thermal treatment being carried out in vacuum, without atmospheric influence, we observed atomic segregation of Pd to the surface. It indicates the lower heat of segregation of Pd atoms in $\text{Pt}_{0.7}\text{Pd}_{0.3}$ nanoparticles if compared to the corresponding bulk alloys.

In summary, S-XPS measurements of the $\text{Pt}_{0.7}\text{Pd}_{0.3}$ nanoparticles were performed before and after thermal treatment under vacuum at 300°C for 20 and 50 min. Our analysis approach was successfully applied to observe a thermally induced atomic rearrangement with the formation of a core–shell structure, resulting in a Pd-enriched shell and a Pt-rich core. The proposed methodology may be employed using one photon energy value, allowing the evaluation of R_{core} and shell thickness from a single S-XPS or even from a conventional XPS measurement. Additional S-XPS measurements using other E_{ph} values would validate the results, requiring the knowledge of the photoemission differential cross section and the mean free path of the photoelectrons for the selected photon energies.

EXPERIMENTAL SECTION

The preparation procedure of the $\text{Pt}_{0.7}\text{Pd}_{0.3}$ nanoparticles was reported in a previous paper.³¹ TEM and HRTEM analyses were carried out on electron microscopes operating at accelerating voltages of 80 kV (JEOL JEM-1200 EXII) and 300 kV (JEOL JEM-3010 URP). For these measurements, a drop of the dispersed $\text{Pt}_{0.7}\text{Pd}_{0.3}$ nanoparticles was spotted on a holey carbon-coated copper grid. HRTEM measurements were performed on as-prepared and annealed (at 300°C for 50 min) nanoparticles. The images were analyzed using the Gatan Digital Micrograph software from which the FT of images was obtained. Energy-dispersive spectroscopy (EDS) analysis (not shown here) in distinct regions merely revealed the presence of Pt and Pd, as expected.

For the S-XPS experiments, about 5 mg of the nanoparticle powder was deposited on a copper stub and introduced into

the SXS beamline³² endstation at the LNLS (Brazilian Synchrotron Light Laboratory). The XP spectra were collected using two distinct incident photon energies $E_{\text{ph}} = 1840$ and 2800 eV, provided by the InSb (111) double crystal monochromator. The hemispherical electron analyzer (Physical Electronics model 10-360) was set to pass energy of 23.5 eV with 0.1 eV energy step and 500 ms/point acquisition time. The overall resolution achieved was about 0.3 eV ($E_{\text{ph}} = 1840$ eV) and 0.9 eV ($E_{\text{ph}} = 2800$ eV). The base pressure of the analysis chamber was 1.3×10^{-9} mbar. The monochromator photon energy calibration was done at the Si K edge (1839 eV) and Mo L₁ edge (2866 eV). An additional calibration of the analyzer's energy was performed using a standard Ag foil (Ag 3d_{5/2} peak at 368.3 eV). We also considered the C 1s peak value of 284.5 eV (adventitious carbon) as a reference in order to verify possible charging effects. All S-XPS measurements were performed at room temperature, using a 45° takeoff angle. The XPSpeak program (version 4.1) was used to fit the XPS results. All peaks were adjusted using a Shirley type background and an asymmetric Gaussian–Lorentzian sum function (with 20 % Lorentzian contribution).

SUPPORTING INFORMATION AVAILABLE Description of the numerical calculation of the differential cross section. This material is available free of charge via the Internet at <http://pubs.acs.org>

AUTHOR INFORMATION

Corresponding Author:

*To whom correspondence should be addressed. Phone number: +55 51 33086525. Fax number: +55 51 33086510. E-mail: jonder@if.ufrgs.br.

ACKNOWLEDGMENT Authors acknowledge the fruitful discussions with Prof. C. S. Fadley. We thank D. O. Silva and Prof. J. Dupont for providing the Pt_{0.7}Pd_{0.3} nanoparticles. We are grateful for the support given by the LNLS staff and J. Boita. This work was funded by CNPq, CAPES, and LNLS (SXS 5734, SXS 6577, SXS 6576, TEM-HR 7386 proposals). F.B. thanks CNPq for his Ph.D. fellowship.

REFERENCES

- (1) Banin, U. Tiny Seeds Make a Big Difference. *Nat. Mater.* **2007**, *6*, 625–626.
- (2) Habas, S. E.; Lee, H.; Radmilovic, V.; Somorjai, G. A.; Yang, P. Shaping Binary Metal Nanocrystals Through Epitaxial Seeded Growth. *Nat. Mater.* **2007**, *6*, 692–697.
- (3) Frenkel, A. I.; Hills, C. W.; Nuzzo, R. G. A View from the Inside: Complexity in the Atomic Scale Ordering of Supported Metal Nanoparticles. *J. Phys. Chem. B* **2001**, *105*(51), 12689–12703.
- (4) Roucoux, A.; Schulz, J.; Patin, H. Reduced Transition Metal Colloids: A Novel Family of Reusable Catalysts?. *Chem. Rev.* **2002**, *102*, 3757–3778.
- (5) Sinfelt, J. H. Supported “Bimetallic Cluster” Catalysts. *J. Catal.* **1973**, *29*, 308–315.
- (6) Yonezawa, T. Synthesis and Characterization of Core–Shell Structured Metals, In *Self-Organized Nanoscale Materials*; Adachi, M., Lockwood, D. J., Eds.; Springer: New York, 2006, pp 251–269.
- (7) Tao, F.; Grass, M. E.; Zhang, Y.; Butcher, D. R.; Renzas, J. R.; Liu, Z.; Chung, J. Y.; Mun, B. S.; Salmeron, M.; Somorjai, G. A. Reaction-Driven Restructuring of Rh–Pd and Pt–Pd Core–Shell Nanoparticles. *Science* **2008**, *322*, 932–934.
- (8) Cheng, D.; Wang, W.; Huang, S. The Onion-Ring Structure for Pd–Pt Bimetallic Clusters. *J. Phys. Chem. B* **2006**, *110*, 16193–16196.
- (9) Bernardi, F.; Alves, M. C. M.; Traverse, A.; Silva, D. O.; Scheeren, C. W.; Dupont, J.; Morais, J. Monitoring Atomic Rearrangement in Pt_xPd_{1-x} ($x = 1, 0.7$, or 0.5) Nanoparticles Driven by Reduction and Sulfidation Processes. *J. Phys. Chem. C* **2009**, *113*(10), 3909–3916.
- (10) Ferrer, D.; Torres-Castro, A.; Gao, X.; Sepúlveda-Guzmán, S.; Ortiz-Méndez, U.; José-Yacamán, M. Three-Layer Core/Shell Structure in Au–Pd Bimetallic Nanoparticles. *Nano Lett.* **2007**, *7*(6), 1701–1705.
- (11) Polak, M.; Rubinovich, L. The Interplay of Surface Segregation and Atomic Order in Alloys. *Surf. Sci. Rep.* **2000**, *38*, 127–194.
- (12) Wang, Y.; Toshima, N. Preparation of Pd–Pt Bimetallic Colloids with Controllable Core/Shell Structures. *J. Phys. Chem. B* **1997**, *101*, 5301–5306.
- (13) Toshima, N.; Harada, M.; Yonezawa, T.; Kushihashi, K.; Asakura, K. Structural Analysis of Polymer-Protected Pd/Pt Bimetallic Clusters as Dispersed Catalysts by Using Extended X-ray Absorption Fine Structure Spectroscopy. *J. Phys. Chem.* **1991**, *95*, 7448–7453.
- (14) Langlois, C. T.; Oikawa, T.; Bayle-Guillemaud, P.; Ricolleau, C. Energy-Filtered Electron Microscopy for Imaging Core–Shell Nanostructures. *J. Nanopart. Res.* **2008**, *10*, 997–1007.
- (15) Schmid, G.; West, H.; Malm, J.-O.; Bovin, J.-O.; Grenthe, C. Catalytic Properties of Layered Gold–Palladium Colloids. *Chem.—Eur. J.* **1996**, *2*(9), 1099–1103.
- (16) Borchert, H.; Haubold, S.; Haase, M.; Weller, H.; McGinley, C.; Riedler, M.; Möller, T. Investigation of ZnS Passivated InP Nanocrystals by XPS. *Nano Lett.* **2002**, *2*(2), 151–154.
- (17) Hwang, B. J.; Sarma, L. S.; Chen, C. H.; Tang, M. T.; Liu, D. G.; Lee, J. F. Depth Profile of Alloying Extent and Composition in Bimetallic Nanoparticles Investigated by In Situ X-ray Absorption Spectroscopy. *Appl. Phys. Lett.* **2007**, *91*, 023108–1–023108–3.
- (18) Tanuma, S.; Powell, C. J.; Penn, D. R. Calculations of Electron Inelastic Mean Free Path. II. Data for 27 Elements Over the 50–2000 eV Range. *Surf. Interface Anal.* **1991**, *17*, 911–926.
- (19) Fiermans, L.; de Gryse, R.; de Doncker, G.; Jacobs, P. A.; Martens, J. A. Pd Segregation to the Surface of Bimetallic Pt–Pd Particles Supported on H-β Zeolite Evidenced with X-Ray Photoelectron Spectroscopy and Argon Cation Bombardment. *J. Catal.* **2000**, *193*, 108–114.
- (20) van den Oetelaar, L. C. A.; Nooitj, O. W.; Oerlemans, S.; Denier van der Gon, A. W.; Brongersma, H. H.; Lefferts, L.; Roosenbrand, A. G.; van Veen, J. A. R. Surface Segregation in Supported Pd–Pt Nanoclusters and Alloys. *J. Phys. Chem. B* **1998**, *102*, 3445–3455.
- (21) Bazin, D.; Guillaume, D.; Pichon, Ch.; Uzio, D.; Lopez, S. Structure and Size of Bimetallic Palladium–Platinum Clusters in an Hydrotreatment Catalyst. *Oil. Gas Sci. Technol.* **2005**, *60*(5), 801–813.
- (22) de Sarkar, A.; Menon, M.; Khanra, B. C. Effect of Metal–Support Interaction on Surface Segregation in Pd–Pt Nanoparticles. *Appl. Surf. Sci.* **2001**, *182*, 394–397.
- (23) Wang, G.; Van Hove, M. A.; Ross, P. N.; Baskes, M. I. Quantitative Prediction of Surface Segregation in Bimetallic Pt–M Alloy Nanoparticles (M = Ni, Re, Mo). *Prog. Surf. Sci.* **2005**, *79*, 28–45.

- (24) Shirinyan, A. S.; Wautelet, M. Phase Separation in Nanoparticles. *Nanotechnology* **2004**, *15*, 1720–1731.
- (25) Massen, C.; Mortimer-Jones, T. V.; Johnston, R. L. Geometric and Segregation Properties of Platinum–Palladium Nanoalloy Clusters. *J. Chem. Soc., Dalton Trans.* **2002**, 4375–4388.
- (26) Hansen, P. L.; Molenbroek, A. M.; Ruban, A. V. Alloy Formation and Surface Segregation in Zeolite-Supported Pt–Pd Bimetallic Catalysts. *J. Phys. Chem. B* **1997**, *101*, 1861–1868.
- (27) Ma, Y.; Balbuena, P. B. Pt Surface Segregation in Bimetallic Pt₃M Alloys: A Density Functional Theory Study. *Surf. Sci.* **2008**, *602*, 107–113.
- (28) Mahfouz, R.; Aires, F. J. C. S.; Brenier, A.; Jacquier, B.; Bertolini, J. C. Synthesis and Physico-Chemical Characteristics of Nanosized Particles Produced by Laser Ablation of a Nickel Target in Water. *Appl. Surf. Sci.* **2008**, *254*, 5181–5190.
- (29) Langlois, C.; Alloyeau, D.; Le Bouar, Y.; Loiseau, A.; Oikawa, T.; Mottet, C.; Ricolleau, C. Growth and Structural Properties of CuAg and CoPt Bimetallic Nanoparticles. *Faraday Discuss.* **2008**, *138*, 375–391.
- (30) Szabo, A.; Paál, Z.; Szász, A.; Kojnok, J.; Fabian, D. J. Surface Composition of Pt–Pd Alloys Treated in Hydrogen. *Appl. Surf. Sci.* **1989**, *40*, 77–83.
- (31) Scheeren, C. W.; Machado, G.; Teixeira, S. R.; Morais, J.; Domingos, J. B.; Dupont, J. Synthesis and Characterization of Pt(0) Nanoparticles in Imidazolium Ionic Liquids. *J. Phys. Chem. B* **2006**, *110*, 13011–13020.
- (32) Tolentino, H.; Compagnon-Cailhol, V.; Vicentin, F. C.; Abbate, M. The LNLS Soft X-ray Spectroscopy Beamline. *J. Synchrotron Radiat.* **1998**, *5*, 539–541.